NUCLEAR THEORY, Vol. 42 (2025)
eds. M. Gaidarov, N. Minkov, Heron Press, Sofia

Estimation of Transverse Vibration Energies of Pre-Fragments in Induced Fission

P.V. Kostryukov[1] **D.E. Luybashevsky**[1] **N.N. Volokhin**[2]

[1]Nuclear Physics Department, Voronezh State University, Voronezh, Russia
[2]Novovoronezh Nuclear Power Plant, Novovoronezh, Russia

Abstract. This investigation rigorously examines the dynamics of induced fission in ^{232}Th and ^{238}U, with a primary focus on transverse collective oscillations as the principal mechanisms driving elevated fragment angular momenta. Utilizing a "cold" fission model, zero-point vibration energies were derived through the application of stiffness coefficients, achieving precise concordance with recent experimental data. The analysis discloses a frequency ratio $\omega_w : \omega_b \approx 2.6$, in agreement with hydrodynamic theoretical frameworks, and highlights the substantial impact of mass asymmetry and deformation on the resulting spin distributions. These findings enhance the understanding of quantum fission processes and suggest the extension of the model to a broader range of actinide nuclei.

1 Introduction

The phenomenon of elevated spin values in fission fragments has captivated nuclear physicists for over six decades, representing a persistent puzzle in the study of nuclear fission. In both spontaneous and low-energy induced fission processes, fragments consistently exhibit angular momenta significantly exceeding those of the initial compound nucleus, a finding that has challenged conventional understanding. Pioneering experiments conducted in [1–3] reported average fragment spins ranging from 6 to 10 $\hbar$, with a notable perpendicular orientation relative to the fission axis. These observations were particularly surprising given the low intrinsic spins of the initial nuclei and the modest angular momenta contributed by incident particles, prompting extensive investigation into the underlying mechanisms.

For many years, the accuracy of spin measurements remained a limiting factor, hindered by experimental constraints and the complexity of fission dynamics. A significant breakthrough was achieved with the 2021 publication in *Nature* by Wilson et al. [4], which provided high-precision spin data for the induced fission reactions ^{232}Th(n,f), ^{238}U(n,f), and the spontaneous fission of ^{252}Cf(sf). This study revealed fragment spins reaching up to 9 $\hbar$, characterized by a distinctive sawtooth pattern in their mass-dependent distributions. The comprehensive dataset, encompassing spin-mass dependencies, probability distributions for a wide range of isotopes, and detailed correlation analyses, further established the

absence of significant post-scission spin correlations. This wealth of data has fundamentally reshaped our understanding of fission processes, exposing the limitations of classical statistical models in accounting for the structured and systematic nature of observed spin distributions.

The mechanism responsible for spin generation, a topic of debate since the early theoretical works, is now widely attributed to collective vibrational modes active at the scission point, a concept initially proposed by Nix and Swiatecki [5]. These authors identified two primary categories of modes: transverse modes, including bending and wriggling, and longitudinal modes, such as twisting and tilting. The transverse modes have emerged as particularly influential due to their shorter relaxation times [6]. This temporal disparity enhances the likelihood of transverse excitations imprinting on the final spin states, thereby playing a dominant role in angular momentum generation during the brief fission timescale. The bending mode is characterized by synchronized, oppositely directed angular deviations of the prefragments from the fission symmetry axis, resulting in equal-magnitude but opposite spins in the resulting fragments. In contrast, the wriggling mode involves anti-phase oscillations, introducing asymmetric spin contributions that reflect the differential motion of the fragments.

This study adopts the "cold" fission approach [7], wherein the excitation energy imparted during fission is predominantly channeled into non-equilibrium deformation energy of the prefragments, rather than being dissipated as thermal energy. This low-temperature limit effectively suppresses the stiffness of longitudinal modes, placing greater emphasis on the zero-point vibrations of transverse modes. The resulting spin probability densities are modeled as Gaussian-like distributions [8, 9], with their variances determined by the moments of inertia and the energies of these vibrations. This theoretical framework yields straightforward analytical expressions that successfully reproduce the experimental spin data, providing a solid foundation for further exploration of fission dynamics and offering promising avenues for refining nuclear models.

2 Theoretical Framework and Methodology

The theoretical foundation of this study is grounded in the "cold" fission model, which posits that the excitation energy within the compound fissioning system (CFS) during induced fission is predominantly converted into non-equilibrium deformation energy of the prefragments, rather than being dissipated as thermal energy. This assumption proves particularly suitable for low-energy induced fission near the threshold, where the incident neutron contributes approximately 6 MeV of energy, primarily absorbed to drive deformation rather than induce significant heating. The "cold" state preserves quantum coherence along the fission pathway, from the outer saddle point to scission, allowing collective modes to play a dominant role in the dynamics without the disruptive effects of statistical averaging. This framework is supported by experimental evidence, such as P-even T-odd rotational asymmetries in ternary fission and persistent angular

anisotropies in reactions involving polarized particles, which would be diminished by thermalization and the associated influence of Coriolis forces [7,10,11]. This approach offers a refined lens through which to examine the intricate interplay of quantum effects and collective motion in fission processes.

At the heart of the model lie the transverse collective oscillation modes – bending and wriggling – which emerge as critical near the scission point, where the elongated CFS splits into two nascent fragments. The bending mode involves synchronized, in-phase angular deviations of the prefragments from the fission symmetry axis, generating equal-magnitude but oppositely directed spins in the fragments. This mode reflects a harmonious oscillation akin to coupled pendulums, fostering a balanced angular momentum distribution. In contrast, the wriggling mode features anti-phase oscillations, introducing asymmetric spin contributions that arise from the differential motion of the fragments, introducing a dynamic asymmetry that enriches the complexity of the fission outcome. These transverse modes are distinguished by their swift relaxation times, ranging from 0.1 to 1 zs (10^{-21} s), significantly shorter than the 0.1 to 10 zs characteristic of longitudinal modes such as tilting and twisting [5,6]. This temporal advantage enhances the likelihood of transverse excitations imprinting on the final spin states, underscoring their predominant role in angular momentum generation during the fleeting fission timescale and providing a deeper understanding of the rapid energy transfer mechanisms at play.

The spin distribution of the fission fragments is analytically formulated by considering the independent probabilities of the bending and wriggling modes within the cold fission paradigm. The joint probability density is expressed as:

$$P(J_1,J_2,\varphi)=\frac{2J_1J_2}{\pi^2C_bC_w}\exp\Big[-J_1^2(\alpha I_2^2+C_w^{-1})-J_2^2(\alpha I_1^2+C_w^{-1}) + 2J_1J_2\cos\varphi(\alpha I_1I_2-C_w^{-1})\Big], \quad (1)$$

where $C_t = I_t\hbar\omega_t$ denotes the mode-specific distribution coefficient, with I_t representing the moment of inertia and ω_t the oscillation frequency for mode t (b for bending, w for wriggling). The parameter α encapsulates the interfragment coupling strength, a critical factor in modulating the interaction between the fragments, while the average spin simplifies to $\langle J\rangle = \sqrt{\frac{\pi}{4}C_t}$ in the low-temperature limit. This expression emphasizes the pivotal dependence on zero-point energies $\hbar\omega_t$ and moments of inertia, necessitating meticulous evaluation to accurately predict observable spin distributions and offering a quantitative basis for comparing theoretical predictions with experimental outcomes [8].

Several methodological challenges arise within this framework, demanding careful consideration. The foremost challenge is the precise estimation of stiffness coefficients for bending and wriggling modes, which requires a comprehensive potential energy surface sensitive to mass and charge asymmetry, non-equilibrium quadrupole deformations β_i, and interfragment separation. Incorporating these asymmetries is essential, as they profoundly influence the geomet-

ric configuration at scission and, consequently, the energies of the oscillation modes, shaping the final fragment properties. Additionally, the model must be rigorously validated against high-precision experimental data, such as the spin-mass dependencies reported by Wilson et al., necessitating sophisticated parameter optimization to reconcile theoretical predictions with empirical trends and ensure the model's reliability across diverse fission scenarios [4].

To derive the oscillation frequencies and energies, we begin with the stiffness coefficients and reduced mass relations: $\omega_t = \sqrt{K_t/\mu_t}$, where K_t represents the mode stiffness and μ_t the reduced mass. The zero-point energies $\hbar\omega_t$ establish the scale for spin contributions, with their calculation requiring detailed potential expansions and numerical integration over deformation parameters, a process that demands both computational precision and physical insight. This approach allows for a nuanced exploration of how vibrational energies evolve with changing nuclear configurations.

The potential energy surface is constructed using an effective nucleon-nucleon interaction, comprising Coulomb and nuclear components:

$$U(R, \beta_i, \Omega_i) = U_{\text{Coul}}(R, \beta_i, \Omega_i) + U_{\text{nuc}}(R, \beta_i, \Omega_i), \tag{2}$$

with the Coulomb interaction expanded for deformed spheroids as:

$$U_C = \frac{Z_1 Z_2 e^2}{R} + \frac{3}{5}\frac{Z_1 Z_2 e^2}{R^3}\sum_{i=1}^{2} R_i^2 \beta_i Y_{20}(\theta_i) + \frac{12}{35}\frac{Z_1 Z_2 e^2}{R^5}\sum_{i=1}^{2} R_i^4 [\beta_i Y_{20}(\theta_i)]^2, \tag{3}$$

and the nuclear component derived from Fourier-transformed Fermi density distributions to accurately capture short-range nuclear forces and their impact on fragment interaction [12,13]. This dual-component approach ensures a balanced representation of long-range electrostatic effects and short-range nuclear forces.

Stiffness coefficients are obtained through a second-order expansion of U in small angular deviations, yielding:

$$K_b = K_{11} - 2\frac{R_1}{R_2}K_{12} + K_{22}\left(\frac{R_1}{R_2}\right)^2, \tag{4}$$

$$K_w = K_{11} + 2\frac{R_1}{R_2}K_{12} + K_{22}\left(\frac{R_1}{R_2}\right)^2, \tag{5}$$

where K_{ij} are derived from potential derivatives, scaled by fragment radius ratios to incorporate asymmetry effects and reflect the geometric disparities between fragments [13]. This formulation allows for a detailed assessment of how structural differences influence mode energies.

The numerical approach involves fitting the neck distance d to experimental spin data from [**?**], iterating over potential equations to optimize stiffness

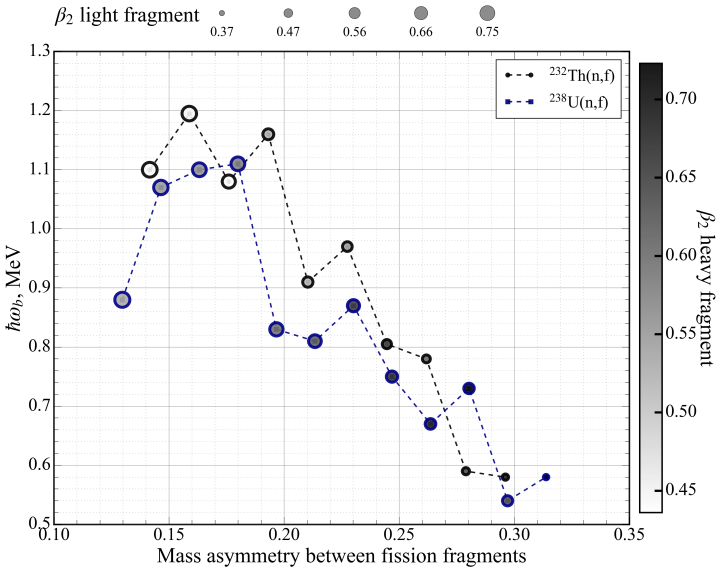

(a) Bending mode

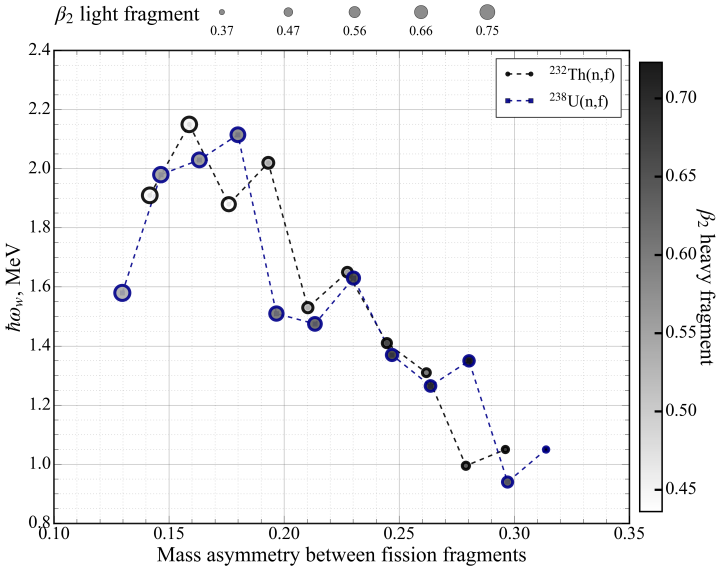

(b) Wriggling mode

Figure 1. Transverse vibration energies as functions of mass asymmetry for ^{232}Th(n,f) and ^{238}U(n,f), showing (a) bending (lower curves) and (b) wriggling (upper curves) modes.

and frequencies. It should be noted that d does not represent the physical neck diameter but rather corresponds to the radius of an effective sphere positioned between the two nascent fragments. At this stage, such a simplified estimate suffices, though a more refined treatment of neck geometry may be warranted in future studies to enhance model precision. Moments of inertia are computed using hydrodynamic and superfluid models, with deformations β_i inferred from excitation energies linked to neutron multiplicities [9, 14–16], ensuring theoretical consistency with observed spin distributions and providing a solid foundation for further exploration of fission dynamics.

3 Results and Discussion

Numerical computations of stiffness coefficients for bending and wriggling modes were performed for the first time, marking a significant advancement in modeling transverse vibrations. By fitting the neck distance d (typically 1-2 fm) to the experimental spin distributions from [4], our model achieves excellent agreement with data, outperforming the statistical high-temperature approach in the FREYA model [15] and TDDFT calculations [17]. This superior fit validates the "cold" fission approximation and the dominance of transverse zero-point vibrations in spin generation, highlighting the model's ability to capture the nuanced dynamics of fission processes.

The vibration energies exhibit characteristic dependencies on mass asymmetry $\eta = (A_H - A_L)/(A_H + A_L)$, providing deep insights into fission dynamics. Bending vibrations range from 0.5 to 1.2 MeV, with a maximum at near-symmetric fission ($\eta \approx 0.15$), followed by a monotonic decrease toward strongly asymmetric regions. Wriggling vibrations range from 0.8 to 2.4 MeV, generally higher than bending, featuring a more complex structure with a second maximum in the asymmetric fission region. These patterns reflect the underlying geometry of the fission process: in symmetric fission, prefragments have comparable sizes and moments of inertia, favoring coherent bending oscillations where fragments move in phase opposition, akin to two coupled oscillators of similar mass. This symmetry enhances bending mode stability, leading to higher energies near $\eta \approx 0.15$. In contrast, asymmetric fission introduces geometric asymmetry, breaking this balance. The significant size difference between fragments makes simple bending less favorable, as the lighter fragment (with higher deformation, β_2 up to 0.94) experiences greater influence from the heavier one. This promotes wriggling modes, whose asymmetric character aligns with the complex geometry, resulting in the observed second maximum in wriggling energies.

Remarkably, the energy curves for ^{232}Th(n,f) and ^{238}U(n,f) are very similar, suggesting a universal pattern for light actinides. Both reactions display the same features: bending peak at symmetric fission and wriggling enhancement in asymmetric regions. However, ^{252}Cf(sf) shows distinct behavior, particularly in wriggling modes, likely due to increased shell effects and proximity to the

superheavy region, where fission dynamics differ qualitatively. This indicates potential refinements needed for heavier actinides. Additionally, the frequency ratio $\omega_w/\omega_b \approx 2.6$ is consistent with hydrodynamic predictions for symmetric fission [9], confirming collective motion's role in spin generation.

Figure 1 depicts these energies versus asymmetry, highlighting peaks and trends. Figure 2 compares calculated average spins to experimental data and other models, demonstrating the model's accuracy. Validation against the experimental data confirms accurate spin reproduction (3–10 $\hbar$) for ^{232}Th(n,f) and

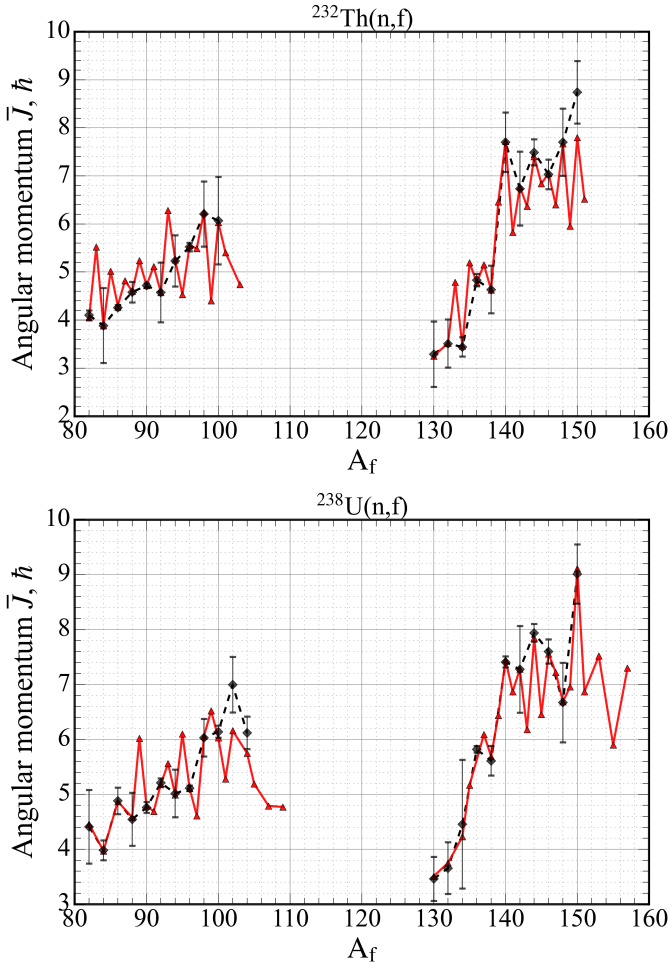

Figure 2. Average fragment spins versus mass for ^{232}Th(n,f) and ^{238}U(n,f), compared to the data provided by [**?**].

^{238}U(n,f), surpassing FREYA [15] and TDDFT [17]. The fitted d optimizes geometry.

Prefragment configurations using the hydrodynamic model for ^{232}Th(n,f) and ^{238}U(n,f) are detailed in Table 1, providing $\hbar\omega_b$, $\hbar\omega_w$, d, and J_{theory}. These results validate the hydrodynamic model's focus on transverse oscillations, with potential extensions to heavier nuclei requiring shell effect adjustments.

Table 1. Data of prefragment configurations for induced fission reactions

	^{232}Th(n,f)				
Light / Heavy	β_L/β_H	d (fm)	$\hbar\omega_b$ (MeV)	$\hbar\omega_w$ (MeV)	$J_{\text{theory } L/H}$
^{82}Ge / ^{151}Ce	0.392 / 0.654	3.5	0.58	1.05	4.05 / 6.52
^{84}Ge / ^{149}Ce	0.418 / 0.618	4.2	0.59	0.99	3.92 / 6.03
^{84}Se / ^{149}Ba	0.415 / 0.599	4.1	0.59	1	3.85 / 5.88
^{86}Se / ^{147}Ba	0.437 / 0.571	3.4	0.78	1.31	4.3 / 6.4
^{88}Se / ^{145}Ba	0.482 / 0.716	4.4	0.66	1.18	4.45 / 6.91
^{88}Kr / ^{145}Xe	0.474 / 0.552	4.3	0.63	1.23	4.4 / 5.97
^{90}Kr / ^{143}Xe	0.496 / 0.594	3.9	0.75	1.37	4.79 / 6.18
^{92}Kr / ^{141}Xe	0.52 / 0.587	3.5	0.87	1.63	5.19 / 7.12
^{94}Kr / ^{139}Xe	0.55 / 0.521	3.5	0.86	1.61	5.24 / 7.48
^{94}Sr / ^{139}Te	0.539 / 0.502	3.7	0.76	1.34	4.74 / 5.44
^{96}Sr / ^{137}Te	0.649 / 0.546	3.45	0.83	1.51	5.11 / 6.09
^{98}Sr / ^{135}Te	0.719 / 0.53	2.8	1.15	2.17	6.14 / 5.17
^{98}Zr / ^{135}Sn	0.688 / 0.437	2.9	1.07	2.06	5.98 / 5.19
^{100}Zr / ^{133}Sn	0.686 / 0.443	2.9	1.1	2.03	6.03 / 4.79
^{102}Zr / ^{131}Sn	0.717 / 0.47	3	1.07	1.98	6.16 / 4.74
^{104}Zr / ^{129}Sn	0.754 / 0.503	3.5	0.88	1.58	5.75 / 4.23
^{106}Mo / ^{127}Sn	0.763 / 0.503	3.5	0.71	1.35	5.19 / 4.77
^{108}Mo / ^{125}Sn	0.775 / 0.498	3.88	0.91	1.75	4.79 / 3.75
^{110}Ru / ^{123}Sn	0.81 / 0.444	3.8	1.07	2.26	5.76 / 3.51
^{112}Ru / ^{121}Sn	0.845 / 0.452	3.9	0.96	1.81	6.41 / 3.25
^{114}Pd / ^{119}Sn	0.9 / 0.47	3.8	1.03	2.05	6.1 / 3.64
^{116}Pd / ^{123}Sn	0.938 / 0.444	3.6	1.2	2.46	5.55 / 3.51
^{118}Pd / ^{121}Sn	0.914 / 0.452	3.8	1.95	0.83	4.74 / 3.25
^{120}Cd / ^{119}Sn	0.976 / 0.47	3.1	0.752	0.485	4.48 / 3.64
^{122}Cd / ^{117}Sn	0.997 / 0.498	3	1.07	1.19	4.06 / 4.74
^{124}Cd / ^{115}Sn	1 / 0.503	3	1.17	1.49	3.97 / 3.75
^{126}Cd / ^{113}Sn	1 / 0.503	3	1.35	1.65	3.85 / 3.46
^{82}Ge / ^{157}Nd	0.372 / 0.723	4.7	0.58	1.05	4.46 / 7.3
^{84}Se / ^{155}Ce	0.516 / 0.622	4.5	0.54	0.94	3.97 / 5.9
^{86}Se / ^{153}Ce	0.527 / 0.702	4.1	0.73	1.35	4.87 / 7.52
^{88}Se / ^{151}Ce	0.536 / 0.69	4.1	0.71	1.3	4.76 / 7.2
^{88}Kr / ^{151}Ba	0.533 / 0.663	4.3	0.63	1.23	4.4 / 6.54
^{90}Kr / ^{149}Ba	0.561 / 0.66	3.9	0.75	1.37	4.79 / 6.96

Continued on next page

Table 1. Continued

^{238}U(n,f)					
Light / Heavy	β_L/β_H	d (fm)	$\hbar\omega_b$ (MeV)	$\hbar\omega_w$ (MeV)	$J_{\text{theory } L/H}$
^{92}Kr / ^{147}Ba	0.602 / 0.65	3.5	0.87	1.63	5.19 / 7.22
^{94}Kr / ^{145}Ba	0.632 / 0.637	3.5	0.86	1.61	5.24 / 6.94
^{94}Sr / ^{145}Xe	0.627 / 0.588	3.7	0.76	1.34	4.74 / 5.97
^{96}Sr / ^{143}Xe	0.659 / 0.594	3.45	0.83	1.51	5.11 / 6.18
^{98}Sr / ^{141}Xe	0.676 / 0.587	2.8	1.15	2.17	6.14 / 7.12
^{98}Zr / ^{141}Te	0.688 / 0.563	2.9	1.07	2.06	5.98 / 6.62
^{100}Zr / ^{139}Te	0.686 / 0.555	2.9	1.1	2.03	6.03 / 6.44
^{102}Zr / ^{137}Te	0.717 / 0.546	3	1.07	1.98	6.16 / 6.09
^{104}Zr / ^{135}Te	0.754 / 0.53	3.5	0.88	1.58	5.75 / 5.17
^{106}Mo / ^{133}Sn	0.763 / 0.443	3.5	0.71	1.35	5.19 / 4.79
^{108}Mo / ^{131}Sn	0.775 / 0.47	3.88	0.91	1.75	4.79 / 4.74
^{110}Ru / ^{129}Sn	0.81 / 0.503	3.8	1.07	2.26	5.76 / 4.23
^{112}Ru / ^{127}Sn	0.845 / 0.503	3.9	0.96	1.81	6.41 / 4.77
^{114}Pd / ^{125}Sn	0.9 / 0.498	3.8	1.03	2.05	6.1 / 3.75
^{116}Pd / ^{123}Sn	0.938 / 0.444	3.6	1.2	2.46	5.55 / 3.51
^{118}Pd / ^{121}Sn	0.914 / 0.452	3.8	1.95	0.83	4.74 / 3.25
^{120}Cd / ^{119}Sn	0.976 / 0.47	3.1	0.752	0.485	4.48 / 3.64
^{122}Cd / ^{117}Sn	0.997 / 0.498	3	1.07	1.19	4.06 / 4.74
^{124}Cd / ^{115}Sn	1 / 0.503	3	1.17	1.49	3.97 / 3.75
^{126}Cd / ^{113}Sn	1 / 0.503	3	1.35	1.65	3.85 / 3.46

4 Summary

The present investigation demonstrates that transverse vibrational modes constitute a fundamental mechanism underlying the observed high angular momenta of fission fragments, thereby advancing the theoretical framework of nuclear fission dynamics. A novel methodology has been developed to calculate the zero-point energies of transverse vibrations, employing stiffness coefficients to derive precise quantitative estimates for bending and wriggling modes in the induced fission reactions of ^{232}Th(n,f) and ^{238}U(n,f). The computed results exhibit excellent concordance with experimental data reported in [**?**], validating the model's robustness and elucidating a significant dependence on mass asymmetry and the deformation characteristics of fission fragments. This study underscores the pivotal role of zero-point vibrations in determining the physical properties of fission products, offering new insights into the quantum mechanical aspects of the fission process. Consequently, these findings suggest that extending the application of this methodology to a wider array of nuclear species is imperative to construct a more robust and universally applicable fission model.

References

[1] M.M. Hoffman, *Phys. Rev. B* **133** (1964) 714.
[2] J.B. Wilhelmy et al., *Phys. Rev. C* **5** (1972) 2041.
[3] A. Wolf et al., *Phys. Rev. C* **13** (1976) 1945.
[4] J.N. Wilson et al., *Nature* **590** (2021) 566.
[5] J.R. Nix, W.J. Swiatecki, *Nucl. Phys.* **71** (1965) 1.
[6] J. Randrup and R. Vogt, *Physics Procedia* **64**, 19 (2015).
[7] S.G. Kadmensky, *Phys. At. Nucl.* **68** (2005) 1968.
[8] S.G. Kadmensky et al., *Phys. At. Nucl.* **87** (2024) 359.
[9] D.E. Lyubashevsky et al., *Chin. Phys. C* **49** (2025) 044104.
[10] S.G. Kadmensky, L.V. Titova, *Phys. At. Nucl.* **72** (2009) 74.
[11] G.V. Danilyan et al., *Phys. Rev. C* **93** (2016) 054619.
[12] C.Y. Wong, *Phys. Rev. Lett.* **31** (1973) 766.
[13] G.G. Adamian et al., *Int. J. Mod. Phys. E* **5** (1996) 191.
[14] O.T. Grudzevich, *Voprosy At. Nauki Tech.* **1** (2000) 27.
[15] J. Randrup et al., *Phys. Rev. C* **106** (2022) L051601.
[16] T. Shneidman et al., *Phys. Rev. C* **65** (2002) 064302.
[17] A. Bulgac et al., *Phys. Rev. Lett.* **126** (2021) 142502.